Nanoscale

ARTICLE

Cationic Polymer Brush-Modified Cellulose Nanocrystals for High-Affinity Virus Binding†

Cite this: DOI: 10.1039/x0xx00000x

Henna Rosilo,[a] Jason R. McKee,[a] Eero Kontturi,[b] Tiia Koho,[c] Vesa P. Hytönen,[cd] Olli Ikkala,[a] Mauri A. Kostiainen*[e]

Received 00th Month XXXX,
Accepted 00th Month XXXX

DOI: 10.1039/x0xx00000x

www.rsc.org/nanoscale

Surfaces capable of high-affinity binding of biomolecules are required in several biotechnological applications, such as purification, transfection, and sensing. Therein, the rod-shaped, colloidal cellulose nanocrystals (CNC) are appealing due to their large surface area available for functionalization. In order to exploit electrostatic binding, their intrinsically anionic surfaces have to be cationized as biological supramolecules are predominantly anionic. Here we present a facile way to prepare cationic CNCs by surface-initiated atom-transfer radical polymerization of poly(*N*,*N*-dimethylaminoethyl methacrylate) and subsequent quaternization of the polymer pendant amino groups. The cationic polymer brush-modified CNCs maintained excellent dispersibility and colloidal stability in water and showed a ζ-potential of +38 mV. Dynamic light scattering and electron microscopy showed that the modified CNCs electrostatically bind cowpea chlorotic mottle virus and norovirus-like particles with high affinity. Addition of only a few weight percent of the modified CNCs in water dispersions sufficed to fully bind the virus capsids to form micrometer-sized assemblies. This enabled the concentration and extraction of the virus particles from solution by low-speed centrifugation. These results show the feasibility of the modified CNCs in virus binding and concentrating, and pave the way for their use as transduction enhancers for viral delivery applications.

Introduction

Cellulosic materials are presently undergoing a paradigm shift from traditional pulp and paper products to high-end sustainable applications. These sophisticated systems are pursued using supramolecular, colloidal and nanocomposite concepts based on native crystalline nanofibers.[1-9] Rod-shaped cellulose nanocrystals (CNCs) are of growing importance for advanced material applications due to their extraordinary mechanical properties, high aspect ratio and surface area, colloidal stability and non-toxic sugar-based chemical composition.[2, 10] Indeed, the additional compatibility of CNCs with water-based systems makes them interesting candidates for biotechnological applications, and studies with biomacromolecules have been presented.[11-13] However, the intrinsically anionic nature of CNCs prepared by sulfuric acid hydrolysis and the likewise negative surface charge of most biomacromolecules prevent the direct use of electrostatic interactions for their binding and assembly, and thus convenient routes for the cationization of CNCs are desirable.

Cationized dissolved or nanofibrillated celluloses have been widely described and recently tested for applications in non-viral gene delivery, drug delivery and non-leaching antibacterial fibers and films.[14-18] In the case of CNCs, the first cationizations were based on the addition of (2,3-epoxypropyl)trimethylammonium chloride to the CNC surface hydroxyl groups.[19-21] Activation of the CNC hydroxyls by strong alkaline treatment before the reaction may simultaneously remove some of the anionic sulfate ester groups, which leads to flocculation of the CNCs.[22] Addition of cationic reagents onto CNCs without the removal of sulfate groups has been realized *via* copper(I)-catalyzed 1,3-dipolar cycloaddition and esterification of imidazolium- and pyridinium-based ionic liquid molecules, producing highly cationic CNCs for ion exchange applications.[23, 24] The copper(I)-catalyzed click reaction has also been used for the attachment of cationic porphyrins to CNCs for the photodynamic inactivation of several bacteria.[25] Despite the presumable electrostatic complexation between the anionic CNCs and a cationic reagent, such observations were not reported.

Development of modern polymerization techniques has opened new pathways for the modification of cellulose. In addition to a thorough chemical coverage of the cellulose backbone, a polymer brush on colloidal CNC particles can introduce tunable or stimuli-responsive properties.[9, 26-28] Poly(*N*,*N*-dimethylaminoethyl methacrylate) (poly(DMAEMA)) is a stimuli-responsive polycation with a pKa of 7.4-7.8 in water.[29] Its dimethylamino groups can be readily converted to permanently cationic quaternary amines by primary alkyl halides. Grafting of poly(DMAEMA) from dissolved cellulose has mostly been studied in the context of stimuli-responsive properties in addition to biomedical and flocculant applications.[30-36] Surface-initiated atom-transfer radical polymerization (SI-ATRP) of DMAEMA producing polymer brush-modified cellulose surfaces or particles has recently expanded from cellulose films to CNCs.[9, 37-40] Here, homopolymerization on CNCs produced short and polydisperse poly(DMAEMA) grafts.[40] However, the morphology and colloidal stability of the water-dispersed poly(DMAEMA)-grafted CNCs were not examined.

Viruses and their capsid proteins have become an indispensable asset for functional nanoscale applications especially in gene delivery and encapsulation of materials.[41-43] Monodispersity of virus capsids allows the preparation of well-defined 3D nanostructures, such as binary superlattices, artificial inclusion bodies and templates for electrode materials.[44-47] In viral delivery applications transduction enhancers are used for overcoming challenges, for example, in concentrating the viral vectors and in attaching the viruses onto cells.[48] A rod-like shape of the carrier and high-affinity binding of viruses by cationic polymers have been shown to significantly improve cell internalization and diffusion-limited transduction.[49, 50] Recently, cationic peptide nanofibrils with a high aspect ratio and high stiffness were reported to form macroscopic complexes with viruses and significantly enhance retroviral gene delivery.[51] In a related concept polydisperse, micrometer long lignin nanotubes were successfully used for plasmid transfection.[52] In this regard, the intercept of biological and synthetic materials, such as chemically modified cellulose nanocrystals, provides novel biocompatible, generic and cost-effective materials for virus binding and delivery applications. To date, fibrillar cellulose and CNCs have, however, only been used for the removal of viruses from solutions by size exclusion filters and antiviral applications.[13, 53, 54]

In this study we first show the efficient and permanent cationization of intrinsically anionic CNCs by SI-ATRP and subsequent chemical modification of the polymer graft pendant groups. In more detail, pristine CNCs were modified with initiator molecules to form colloidal macroinitiators for subsequent grafting of poly(DMAEMA) from the CNC surface. The polymer brush-modified CNC-*g*-P(DMAEMA) were further quaternized with methyl iodide, producing permanently cationic CNC-*g*-P(QDMAEMA). Thorough characterization of the particles and the grafted polymer proved the presence of a highly cationic polymer brush on the CNCs. Next, as a first example of a high affinity and assembly formation of cationic CNCs with viruses, we demonstrate the electrostatic binding of the CNC-*g*-P(QDMAEMA) to cowpea chlorotic mottle virus (CCMV) and norovirus-like particles (NoV-VLP) by dynamic light scattering, gel electrophoresis and electron microscopy. Furthermore, we show the efficient concentration and extraction of virus particles with CNC-*g*-P(QDMAEMA) from solution by low-speed centrifugation. CCMV is a plant virus with a 28 nm outer diameter, that is often used in nanotechnology-based applications and as a model system due to its excellent stability and reversibility of the virus capsid self-assembly.[55] NoV-VLPs of the GII.4 type are non-pathogenic recombinant capsid protein cages void of the native RNA, yet with a similar morphology as the native capsid, and a diameter of 40 nm. NoV-VLP has previously been used for example in vaccine development.[56] Both virus particles have an icosahedral symmetry and a negatively charged outer surface readily available for electrostatic self-assembly. The concept is general and suitable for the assembly of other viruses, bacteria[57] and anionic materials.

Experimental section

Materials

All chemicals, except the ones specifically stated below, were purchased from Sigma-Aldrich and used without further purification. DMAEMA monomer was purchased from Sigma-Aldrich and purified by running it through basic alumina. Ethanol (99.6%) was purchased from Altia and used as received. Uranyl acetate was purchased from Electron Microscopy Sciences. 6 X DNA Loading Dye was purchased from Fermentas.

Pristine cellulose nanocrystals

CNCs were prepared from ground Whatman 541 ashless filter paper by sulfuric acid hydrolysis and characterized as previously published.[8, 58] Yield of the CNCs was 35%. The surface charge of the CNCs was 360 meq/kg as determined by conductometric titration, corresponding to a sulfate ester degree of substitution of approximately 0.1.[59]

Synthesis of α-bromoisobutyryl bromide (BriBBr) modified CNCs

Freeze-dried pristine CNCs (1000 mg, 6.2 mmol of glucose units) were first modified *via* chemical vapor deposition (CVD) with BriBBr for 48 hours. The crude CVD product was purified *via* consecutive wash and centrifugation cycles (2 x DMF, 2 x acetone, 2 x ethanol and 2 x 1,4-dioxane) and soxhlet extraction with DCM for 48 hours. The BriBBr-modified CNCs (CNC-iBBr) (780 mg) were dispersed in dry DMF (80 mL) using stirring and mild sonication. After purging the system with nitrogen, pyridine (2.0 mL, 24.8 mmol) and 4-dimethylaminopyridine (DMAP) (50 mg, 0.41 mmol) were added to the suspension. The reaction mixture was then cooled to 0 ^{o}C and BriBBr (2.0 mL, 16.2 mmol) was added dropwise. After 30 minutes, the reaction was allowed to warm up to room

temperature (21 °C) and stirred for a further 48 hours. CNC-iBBr were purified *via* consecutive wash and centrifugation cycles with different organic solvents (3 x DMF, 2 x MeOH and 2 x 1,4-dioxane) and then soxhlet-extracted with DCM for 48 hours. The purified CNC-iBBr's were dispersed in 1,4-dioxane and freeze-dried. Elemental analysis found (mass-%): Br: 4.14.

SI-ATRP of DMAEMA

DMAEMA (4082.2 mg, 25.97 mmol) was added into a suspension of CNC-iBBr (100 mg, 0.57 mmol, n(Br) 0.052 mmol) in dry DMF (3 mL). The suspension was purged with nitrogen for 15 minutes. Next, Cu(I)Br (8.0 mg, 0.056 mmol) was quickly added into the reaction flask. After another 15 minutes of nitrogen bubbling, hexamethyltriethylenetetramine (HMTETA) (23.9 mg, 0.104 mmol) and ethyl α-bromoisobutyryl bromide (EBiB) as the sacrificial initiator (5.06 mg, 0.026 mmol) were dissolved in dry DMF (2 mL), and added *via cannula* into the reaction flask. The flask was then stabilized in an oil-bath at 70 °C and stirred for 240 minutes, with a batch of the reaction mixture extracted after 120 min. Finally, the reaction was terminated by quenching with oxygen and cooling the reaction flask to room temperature (21 °C). The crude CNC-graft (CNC-*g*-P(DMAEMA)) was precipitated in methanol, followed by several re-dispersion and centrifugation cycles in different organic solvents (3 x MeOH, 2 x DMF and 2 x 1,4-dioxane). Finally, CNC-*g*-P(DMAEMA) was dispersed into 1,4-dioxane and freeze-dried. The free poly(DMAEMA) resulting from the sacrificial initiator was extracted during the centrifugation cycles, dialyzed against methanol and freeze-dried.

Quaternization of CNC-*g*-P(DMAEMA) with methyl iodide (MeI)

CNC-*g*-P(DMAEMA) (300 mg) and MeI (2 mL) were both dispersed into Milli-Q water (30 mL) and vigorously stirred for 7 days. The crude CNC-*g*-P(QDMAEMA) was first purified by evaporating excess MeI under vacuum. The subsequent CNC-*g*-P(QDMAEMA) dispersion was then purified *via* consecutive wash and centrifugation cycles in water (x4) and finally freeze-dried from water to yield CNC-*g*-P(QDMAEMA) as a yellow powder. Elemental analysis found (mass-%): C: 36.67, N: 4.20, I: 37.9.

Cowpea chlorotic mottle virus (CCMV)

Native CCMV were prepared as reported previously.[60, 61] CCMV stock solution was 10 mg/mL in an acetate buffer (100 mM NaAc, 10 mM EDTA, 10 mM NaN_3, pH 5) and stored at +4 °C.

Norovirus-like particles (NoV-VLP)

NoV-VLPs were produced in *Spodoptera frugiperda* Sf9 insect cells using baculovirus as a vector. Preparation of recombinant baculovirus carrying norovirus GII.4 in genome is described earlier.[62] The production and anion-exchange chromatographic purification of VLPs was performed as described previously.[63] The resulting VLPs were dialyzed to 20 mM NaH_2PO_4 (pH 6), 500 mM NaCl stock solution in concentration of 0.98 mg/mL, analyzed using SDS-PAGE and stored at +4 °C. For measurements, part of the particles were moved to Milli-Q water and concentrated to 3 mg/mL stock solution.

Elemental analysis

Elemental analyses were performed by Mikroanalytisches Labor Pascher, Germany.

Fourier transform infrared spectroscopy (FTIR)

Transmission spectra were recorded with Nicolet 380 FT-IR spectrometer (Thermo Fisher Scientific) using an attenuated total reflection (ATR) cell by averaging 64 spectra with 4 cm^{-1} resolution. Air background spectra were acquired before each set of measurements. All samples were vacuum dried before measurements.

Nuclear magnetic resonance (^{1}H NMR)

^{1}H NMR spectra were measured with a Bruker AVANCE 400 MHz spectrometer (Bruker) with a 5 mm BBFO probe using deuterated chloroform ($CDCl_3$) as the solvent. Chemical shifts were presented in ppm downfield using tetramethyl silane (0 ppm) as an internal standard.

Gel permeation chromatography (GPC)

GPC was performed with a Waters chromatograph equipped with three Styragel columns (HR2, HR4, HR6) and a Waters 410 differential refractometer (Waters Instruments). DMF/LiCl (1 mg/mL) was used as an eluent with a flow rate of 0.8 mL/min. Poly(methyl methacrylate) (PMMA) (PSS Polymer Standards Service GmbH) was used for calibration.

Atomic force microscopy (AFM)

AFM imaging was conducted with Dimension 5000 scanning probe microscope (Veeco) with a Nanoscope V controller (Digital Instruments) in tapping mode. Images were processed with Gwyddion 2.22 software. NSC15/AlBS tips (Micromash) with a typical resonance frequency of 325 kHz and a tip radius under 8 nm were used. Scanning rate was 1 Hz. Sonicated CNC-*g*-P(QDMAEMA)s (0.5 mg/mL) were spin coated (5000 rpm) on freshly cleaved mica.

Transmission electron microscopy (TEM)

Transmission electron micrographs were imaged in bright field mode with Tecnai 12 Bio Twin instrument (FEI), operating at an accelerating voltage of 120 kV, and recorded with UltraScan 1000 CCD camera (Gatan). Images were processed with Digital Micrograph 3.8.2 for GMS 1.3.3 (Gatan) and ImageJ 1.47v softwares. Samples were prepared on holey carbon film coated 200 mesh copper grids (Electron Microscopy Sciences). 3 µL drop of the sample dispersion was placed on the grid and left standing for 60 s, after which excess solution was blotted away with filter paper. For negative staining, 3 µL drop of 0.5% uranyl acetate in Milli-Q water was subsequently placed on the

grid for 60 s and blotted away. The samples were dried in air overnight before imaging or imaged right away.

CNC-*g*-P(QDMAEMA) samples were prepared in water (0.1 mg/mL) and bath sonicated before moving the samples on TEM grids. CCMV sample was prepared from salt free DLS solution (0.06 mg/mL). NoV-VLP samples were prepared from stock solutions without salt and with 500 mM NaCl. Complexes of CNC-*g*-P(QDMAEMA) and CCMV were prepared right before imaging by mixing CNC-*g*-P(QDMAEMA) (0.1 mg/mL in water) and CCMV (0.06 mg/mL in water) at 1:1 v/v ratios. Complexes of CNC-*g*-P(QDMAEMA) NoV-VLP were cast on TEM grids from DLS samples after the titrations (see below).

Dynamic light scattering (DLS), electrophoretic mobility and ζ-potential of CNC and CNC-*g*-P(QDMAEMA)

Zetasizer Nano S analyzer (Malvern Instruments) with a He-Ne laser of 633 nm was used for measuring the particle size distributions, electrophoretic mobilities and ζ-potentials of pristine CNCs and CNC-*g*-P(QDMAEMA)s at 173˚ backscattering angle. Disposable 1.5 mL semi-micro PMMA cuvettes (Plastibrand) were used for DLS measurements and folded capillary cells (Malvern) for ζ-potential measurements. CNC and CNC-*g*-P(QDMAEMA) (0.5 mg/mL in Milli-Q water) were sonicated and filtered through 0.45 μm filters (Corning) immediately before measuring at 25 ˚C. DLS results are an average of three measurements with 10 measurement runs of 10 seconds each. Mobility values were converted to ζ-potentials using the Smoluchowski equation and reported values are an average of four measurements with 50 measurement runs.

DLS of complexes of CNC-*g*-P(QDMAEMA) with CCMV and NoV-VLP

Instrument details were as above. CNC-*g*-P(QDMAEMA) in Milli-Q water (0.1 mg/mL) were filtered with 0.45 μm filters (Corning) and bath sonicated before the measurement. CCMV stock solution (10 mg/mL) was diluted to 0.06 mg/mL with Milli-Q water and 500 μL of the solution was taken for the titration. NoV-VLP sample at 0 mM NaCl was diluted from the stock solution (3 mg/mL, 0 mM NaCl) to 0.06 mg/mL with Milli-Q water, and 500 μL of the solution was taken for the titration. NoV-VLP sample at 200 mM NaCl was diluted from the stock solution (0.98 mg/mL, 20 mM NaH_2PO_4, 500 mM NaCl) to 0.06 mg/mL and 200 mM NaCl, and 500 μL of the solution was taken for the titration. DLS results are an average of three measurements with 6 measurement runs of 10 seconds each at 25 ˚C. Concentrations were corrected by taking into account the volume changes after CNC-*g*-P(QDMAEMA) additions. Size values presented in Fig. 3 are based on the volume-average distributions.

Gel electrophoresis

Gel electrophoresis was carried out with PowerPac Basic equipment (Bio-Rad). Agarose gel was prepared by dissolving 1 g of agarose into 100 mL of acetate buffer (10 mM NaAc, 10 mM Acetic acid, 1 mM EDTA, pH 5) and stained with 80 μL of ethidium bromide solution (0.625 mg/L). CCMV concentration was 50 mg/L in every sample and CNC-*g*-P(QDMAEMA) concentration varied from 0 to 20 mg/L. 1 μL of 6 X Loading Dye was used to stain the samples. 15 μL of each sample solution was pipetted into the agarose gel wells. The gel was run with a constant voltage of 90 V for 45 minutes and imaged with Gel Doc EZ imaging system with Image Lab 3.0.

Fluorescence spectroscopy

Fluorescence spectra were recorded using a QuantaMaster 40 spectrofluorometer (Photon Technology International). A double excitation monochromator was used in the measurements to decrease the stray light level and the slits in excitation and emission monochromators were set to 5 nm. Spectra were recorded using standard 90° measurement geometry without filters in excitation or emission channel. Spectra were corrected by subtracting a blank sodium acetate buffer background and by using instrument's excitation and emission corrections provided by the manufacturer.

Preparation of fluorescein-tagged CCMV (CCMV-Fluos) and concentration of CCMV-Fluos by centrifugation

CCMV was tagged with 5(6)-carboxyfluorescein *N*-hydroxysuccinimide ester (Fluos) as previously published,[64] and CCMV-Fluos (0.003 mg/mL) was stored in the sodium acetate buffer (1 mM, pH 4.9) at +4 °C. DLS characterization of CCMV-Fluos was performed as with pure CCMV (see above). Fluorescence spectrum of CCMV-Fluos (600 μL, 0.003 mg/mL) in sodium acetate buffer (1 mM, pH 4.9) was first recorded. Bath sonicated CNC-*g*-P(QDMAEMA) in water (0.4 μL, 0.1 mg/mL) were added, the dispersion was mixed with a micropipette and centrifuged at 9000 rpm (7439 x *g*), 10 min. Supernatant was recovered and 20 μL of the virus concentrate was discarded at each step. The cycle was repeated still two times with total amount of added CNC-*g*-P(QDMAEMA) was 1.2 μL. For the control measurements of pure CCMV-Fluos, only the centrifugations and supernatant recoveries were performed.

Results and Discussion

Cationic CNC-*g*-P(QDMAEMA)s were prepared by grafting poly(DMAEMA) by SI-ATRP from the cellulose nanocrystal surface and quaternizing the ternary dimethylamino pendant groups of the polymer with methyl iodide (Fig. 1a). First, initiator-modified CNCs (CNC-iBBr) were prepared by covalently esterifying the initially anionic CNCs with BriBBr. We used a two-step method to ensure a high density of initiating sites on the CNCs. Freeze-dried CNCs were first modified *via* CVD with volatile BriBBr to improve the dispersibility of the CNCs into DMF, as the reaction with BriBBr was continued in DMF under regular esterification conditions.[65] Elemental analysis of the CNC-iBBr gave a bromine content of 4.14 wt%, corresponding to a degree of substitution of approximately 0.27 at the CNC surface (see ESI† for calculation).

Surface modification of the colloidal macroinitiator CNC-iBBr was continued by SI-ATRP of DMAEMA from the crystal surface in DMF, a polar and well-dispersing solvent for CNC-iBBr. In addition to CNC-iBBr, the polymerization also contained EBiB as a sacrificial initiator. Molar ratios of [monomer]/[initiator]/[sacrificial initiator] were [500]:[1]:[0.5]. High monomer-to-initiator ratios, in SI-ATRP, provide longer polymer brushes at lower conversions and, more importantly, limit the amount of unwanted termination and cross-linking reactions.[66] Sacrificial initiators used in SI-ATRP allow for better control over the polymerization as their presence increases the concentration of Cu(II) deactivator species in the reaction, providing slower and more uniform growth of the grafted polymer chains.[66, 67] Furthermore, the use of a sacrificial initiator has been shown to decrease the polydispersity index (PDI) in SI-ATRP of DMAEMA from cellulose films.[37] In the case of convex nanoparticles, such as CNCs, where polymer chain confinement during polymerization is less prominent than for concave or flat surfaces, the molecular weight and PDI of the free homopolymer will most likely correspond well with the surface-initiated grafts, and thus characterization of the CNC-grafted polymer could reliably be performed *via* characterization of the free poly(DMAEMA).[28] Additionally, removal of polymer chains from CNC surface for characterization is often challenging without simultaneously degrading the polymer, unless the initiator molecule is specifically designed for degradation under mild conditions, as has been shown also for cellulose-grafted poly(DMAEMA).[31, 35, 36]

An aliquot of the SI-ATRP reaction mixture was extracted at 120 minutes into the 240 min reaction. Monomer conversions were determined by ^{1}H NMR for both the 120 and 240 min samples by comparing the monomer vinyl signals (5.49 ppm and 6.04 ppm) to the polymer pendant methyl signal (0.83-0.98 ppm) (Fig. 1b, shown for the 240 min sample, see Fig. S1† for other spectra and spectral assignments). Based on the conversions calculated from ^{1}H NMR, the number averaged molecular weights (M_n) of poly(DMAEMA) were 21 000 g/mol and 24 000 g/mol at 120 and 240 minutes, respectively. The polymerization leveled off at approximately 35% conversion (Fig. S2†). A low conversion is typical for SI-ATRP reactions and conversions under 40% are desirable in order to avoid unwanted side reactions.

PDIs of the poly(DMAEMA) grafts were determined by studying the sacrificial poly(DMAEMA) homopolymers by DMF-GPC using PMMA standards. According to the DMF-GPC chromatograms, the PDIs were 1.19 and 1.26 for the 120 min and 240 min samples, respectively. These PDIs were slightly larger than for a fully controlled ATRP, yet lower than in previous studies, where values between 1.38 and 1.62 for poly(DMAEMA) cleaved by acid hydrolysis from cellulose surface were reported, although it should be noted that acid treatment can increase the polydispersity to some extent.[37, 40] The molecular weights obtained from DMF-GPC using PMMA standards corresponded well with the number averaged molecular weights (M_n) calculated from ^{1}H NMR.

The CNC-*g*-P(DMAEMA) were further modified by quaternizing them with methyl iodide in pure water. Initially, CNC-*g*-P(DMAEMA) did not disperse well into neutral water, however, with increasing degrees of quaternization their compatibility with water and thus the availability of the pendant dimethylamino groups to the reagent increased. Due to the low aqueous solubility of MeI, a long reaction time was used to guarantee a thorough quaternization of the material and good dispersibility in water. Despite the higher polydispersity of the 240 min sample, this latter batch of CNC-*g*-P(QDMAEMA) was chosen for the following characterizations and complexation studies due to its better dispersibility in water.

Success of the quaternization reaction was confirmed by FTIR, elemental analysis and ζ-potential measurements. FTIR of CNC-*g*-P(QDMAEMA) (Fig. 1c) predominantly showed a typical poly(QDMAEMA) spectrum with signals at 1142 cm^{-1} (-C-N<), 1475 cm^{-1} (-CH_2-), 1724 cm^{-1} (>C=O) and 2950 cm^{-1} (-CH_2-, -CH_3). The -$N(CH_3)_2$ signals at 2700-2800 cm^{-1} were not visible after quaternization. Cellulose signals were only weakly visible, which is typical for profoundly brush-modified celluloses.[9, 36, 40] Elemental analysis of CNC-*g*-P(QDMAEMA) gave a molar N:I ratio of 1:1 indicating that the poly(QDMAEMA) was fully quaternized. Considering the full quaternization, the molecular weights of the poly(QDMAEMA) iodine salts for the 120 min and 240 min samples were calculated to be approximately 40 000 and 46 000 g/mol, respectively.

By this synthesis route, we were able to efficiently shield the anionic sulfate ester groups on the CNCs by grafting a weakly cationic polymer brush from the CNCs before quaternization. This reduced the possibility of complexation between the anionic CNCs and a cationic reagent and produced a thick layer of permanent and pH-independent cationic charges on the CNCs.

Nature of the surface charges on pristine CNCs and CNC-*g*-P(QDMAEMA)s was characterized by measuring the electrophoretic mobilities and ζ-potentials of the particles in water at 0.5 mg/mL concentration (Table 1). Pristine CNCs had an electrophoretic mobility of -3.20 x 10^{-8} m^2/Vs due to the anionic sulfate ester groups. The cationic CNC-*g*-P(QDMAEMA)s, on the other hand, showed a positive mobility of the same order, 2.96 x 10^{-8} m^2/Vs . These mobility values were transformed to ζ-potential values giving approximately -41 mV and +38 mV for the pristine CNCs and CNC-*g*-P(QDMAEMA)s, respectively. It should be noted that the ζ-potential values can be accurately derived only for spherical particles, and should thus be used only for comparative purposes indicating that both pristine and cationized CNCs were highly charged with opposite surface charges.

Dynamic light scattering was used to estimate the apparent hydrodynamic diameter (D_h) of CNC particles before and after polymer grafting. DLS measurements of pristine and modified CNCs provided near monodisperse particle size distributions with D_h of 93 nm and 202 nm, respectively (Table 1, Fig. S3† for curve profiles). The grafted poly(QDMAEMA) brush on the CNCs was expected to be highly hydrated, and consequently

the D_h of the CNC-*g*-P(QDMAEMA) was observed to be significantly larger than for the pristine CNCs. As in the case of the ζ-potentials, the D_h values should not be understood as exact maximal dimensions of the rod-like CNCs or CNC-*g*-P(QDMAEMA), rather, they highlight subtle change in diffusion properties after chemical modification of the CNCs, and that no apparent aggregation occurred at low concentrations.

Table 1. Electrophoretic mobilities, ζ-potentials and hydrodynamic diameters (D_h) of pristine CNCs and CNC-*g*-P(QDMAEMA) in water (0.5 mg/mL).

Component	Electrophoretic mobility (10^{-8} m^2/Vs)	ζ-potential (mV)	Hydrodynamic diameter D_h (nm)
CNC	-3.20±0.05	-40.8±0.6	93±1
CNC-*g*-P(QDMAEMA)	2.96±0.05	37.7±0.6	202±8

After quaternization, the morphology and integrity of the nanocrystals and the quality of their dispersion in water was studied by AFM, TEM and visual inspection (Fig. 2). AFM of bath sonicated CNC-*g*-P(QDMAEMA)s spin coated on mica revealed individual, well-separated nanocrystals with only a few larger aggregates (Fig. 2a). Also in TEM, individual CNC-*g*-P(QDMAEMA)s were clearly visible (Fig. 2b). Pristine CNCs usually possess a very smooth appearance in TEM, however, the surface of the CNC-*g*-P(QDMAEMA) appeared significantly rougher, suggesting the presence of a polymer brush on the crystals (Fig. 2b-c).[65] In water, CNC-g-P(QDMAEMA) formed clear and stable dispersions even at high concentrations (5 mg/mL) without sonication, as observed by eye (Fig. 2d). The CNC-*g*-P(QDMAEMA) in solution are thus present as individual rod-shaped particles with an exceptionally high cationic surface area available for efficient binding of anionic entities.

The ability of CNC-*g*-P(QDMAEMA) to bind CCMV and NoV-VLP by electrostatic interactions was examined by DLS and in the case of CCMV, also by gel electrophoresis. Outer diameter of the CCMV is approximately 28 nm and the isoelectric point (pI) of the capsid is 3.8 with the negative charges situated at patches on the capsid surface.[68] For NoV-VLP, the diameter and pI are slightly larger, approximately 40 nm and 5.6, respectively. Since the NoV-VLP capsid is assembled without the viral RNA molecule, electrostatic interactions between the RNA and the interior of the capsid have been eliminated, and the stability of the capsid can differ from that of the native norovirus.[69] Due to the suspected instability of the virus capsid at low salt concentrations, complexation of the NoV-VLP with CNC-*g*-P(QDMAEMA) was consequently conducted at two salt concentrations, in pure water and at 200 mM NaCl. As for the more stable CCMV, only complexation in pure water was examined to demonstrate the binding at its most efficient level.

During DLS measurements, the virus solutions were titrated with a CNC-*g*-P(QDMAEMA) dispersion and formation of complexes was detected by following the changes of the volume-averaged size distributions. For the pure CCMV solution, that is, in the absence of salt, a near monodisperse size distribution with a D_h of 27 nm was observed (Fig. 3a). The diameter corresponded well to the expected 28 nm. When CNC-*g*-P(QDMAEMA) was added to the solution, the intensity of free CCMV started to decrease rapidly and a second peak resulting from larger complexes of CNC-*g*-P(QDMAEMA) and CCMV appeared. Fig. 3b presents the decrease of the free CCMV intensity and the changes in the secondary assembly size when the CNC-*g*-P(QDMAEMA) concentration was increased. At a CNC-*g*-P(QDMAEMA) concentration of 1.6 mg/L (2.7% w/w of CNC-*g*-P(QDMAEMA)/CCMV), free CCMV was no longer detectable. Size of the secondary assemblies, however, remained at 200-500 nm until the concentration of CNC-*g*-P(QDMAEMA) was approximately 5 mg/L (10% w/w), after which the assembly size increased abruptly to a few micrometers. This suggests that the CCMV particles first assemble around single CNC-*g*-P(QDMAEMA) nanorods, and only after a certain threshold in the CNC-*g*-P(QDMAEMA) concentration, the virus-coated CNC-*g*-P(QDMAEMA) assemble into larger aggregates.

By contrast, NoV-VLPs in a salt-free solution showed in DLS a near monodisperse hydrodynamic diameter of 74 nm instead of the expected 40 nm, suggesting that the particles were somewhat aggregated or swollen (Fig. 3d). In a salt-free solution the complexation of CNC-*g*-P(QDMAEMA) with NoV-VLP was even more efficient than with CCMV. Indeed, the free NoV-VLP peak was not visible beyond CNC-*g*-P(QDMAEMA) concentration of 0.8 mg/L (1.3% w/w) (Fig. 3e). Due to the higher pI and less negative surface of the NoV-VLP compared to CCMV, weaker binding to CNC-*g*-P(QDMAEMA) was expected. Effectiveness of the complexation probably arises from the inherent instability or aggregation tendency of the NoV-VLPs in salt-free solutions. However, the secondary assemblies remained smaller in size throughout the titration when compared to complexation with CCMV, at around one micrometer. The absence of larger assemblies is indicative of a different mode of binding than with the CCMV, probably due to the less negatively charged surface of the NoV-VLP.

At a NaCl concentration of 200 mM, the D_h of NoV-VLP was initially 45 nm and accordingly closer to the expected value of 40 nm. However, due to the charge screening effect of the salt, the binding of CNC-*g*-P(QDMAEMA) to NoV-VLP was weaker and efficient complex formation was only observed at higher CNC-*g*-P(QDMAEMA) concentrations (Fig. 3f). Free NoV-VLP was not detectable beyond CNC-*g*-P(QDMAEMA) concentration of 26.5 mg/L (60% w/w). Similarly to the complexes in the salt-free solution, the secondary assembly size remained at around one micrometer.

Thus very low amounts of the CNC-*g*-P(QDMAEMA) were needed to fully bind virus particles in solution. Characteristically for electrostatic binding, the complexation efficiency and the nature of the secondary assemblies were dependent on the salt concentration of the solution and surface

properties of the viruses. Nevertheless, these results are promising for further studies with various anionic capsids.

Gel electrophoresis was further used for examining the binding between CNC-*g*-P(QDMAEMA) and CCMV. Both CNC-*g*-P(QDMAEMA)-bound and free CCMV were observable on the gel and formation of larger assemblies could be detected from the decreased mobility of CCMV (Fig. 3c). At CNC-*g*-P(QDMAEMA) concentrations above 5 mg/L, or 10% w/w, free CCMV was no longer detectable. However, part of the secondary assemblies were still able to migrate within the gel until a CNC-*g*-P(QDMAEMA) concentration of 12.5 mg/L (25% w/w) was achieved, confirming the formation of even larger aggregates. This is in good agreement with the DLS results, where the size of the secondary assemblies remained low even in the absence of free CCMV, and abruptly increased at 10% w/w CNC-*g*-P(QDMAEMA) concentration. Since the gel was run in an acetate buffer solution, the electrostatic binding was slightly weaker than in pure water and higher amounts of CNC-*g*-P(QDMAEMA) were needed for complexation.

Binding of the CNC-*g*-P(QDMAEMA) to the virus particles was directly imaged by TEM (Fig. 4). According to the TEM images, native CCMV particles were individually dispersed in water (Fig. 4a). For imaging the complexes of CCMV and CNC-*g*-P(QDMAEMA), the components were mixed at a mass ratio 1:1.7 using the dispersions prepared for DLS titrations. Images show that CCMV was bound to the CNC-*g*-P(QDMAEMA) particles in a fashion where several viruses covered one CNC-*g*-P(QDMAEMA), and some of the assemblies gathered together into larger aggregates (Fig. 4b).

In the case of the NoV-VLP, TEM samples were prepared from both the 0 mM NaCl solution prepared for DLS measurements and the stock solution with 500 mM NaCl (Fig. 4c, Fig. S4† for images at 0 mM NaCl). In the solution with high salt concentration the NoV-VLPs were well-dispersed and showed intact capsid morphology. The average diameter was close to the theoretical value, approximately 46 nm. Complexes of NoV-VLP and CNC-*g*-P(QDMAEMA) were imaged from the DLS samples after the titrations at 0 mM and 200 mM NaCl. At the higher salt concentration, the virus-like particles retained their size and morphology during the complexation with CNC-*g*-P(QDMAEMA) (Fig. 4d). However, less virus particles were bound per nanocrystal than in the case of CCMV. Tightly packed aggregates were not observed and instead the larger assemblies resembled network-like structures. In pure water, the average NoV-VLP diameter expectedly increased slightly to about 55 nm (Fig. S4a†). The virus particles also appeared to be more sensitive to aggregation and even disintegration, as deformed particles were visible in TEM especially after longer storage times. In the absence of salt, part of the NoV-VLPs seemed to disintegrate in contact with the CNC-*g*-P(QDMAEMA) (Fig. S4b†). It is possible that the ionic binding between the NoV-VLP and cationic CNCs further destabilized the NoV-VLPs, causing them to fall apart leaving only disjoint capsid proteins on the CNC-*g*-P(QDMAEMA).

A low concentration of virus vectors has been a long-standing obstacle in the realization of efficient viral gene transduction applications, and usually the vector concentration has to be increased by laborious ultracentrifugations.[70] Formation of micrometer-sized complexes between the viruses and CNC-*g*-P(QDMAEMA) in solution enabled us to easily concentrate and extract CCMV by low-speed centrifugation. In order to demonstrate this, CCMV was first tagged with a fluorescein dye (CCMV-Fluos). Integrity of the CCMV-Fluos was examined by DLS, showing a negligibly broader size distribution than for the pure CCMV, with a D_h of 34 nm, and confirming the absence of prominent aggregation (Fig. 5a). A solution of the fluorescently tagged CCMV was then titrated with CNC-*g*-P(QDMAEMA), centrifuged for 10 min at 9000 rpm (7439 x *g*) and at each step the supernatant was recovered for fluorescence spectroscopy (Fig. 5b). As seen in the DLS studies, the formation of secondary assemblies was very abrupt. Only 4.4 % (w/w) (0.8 µL) of CNC-*g*-P(QDMAEMA) was required to decrease the fluorescence of the supernatant to 12% of the initial fluorescence of CCMV-Fluos at 512 nm. However, when CCMV-Fluos alone was subjected to similar centrifugation cycles, the fluorescence intensity of the recovered supernatant did not decrease, confirming that concentrating CCMV alone is not possible by low-speed centrifugation (Fig. 5c). Thus the virus-coated, rod-shaped secondary assemblies can be effortlessly collected and transported to further tests for cellular delivery and viral gene delivery applications. Furthermore, electrolyte-gated release offers a straightforward method for recovering the bound viral particles.

Conclusions

Cationic, poly(QDMAEMA) brush-modified cellulose nanocrystals were prepared from intrinsically anionic CNCs by SI-ATRP of DMAEMA from the crystal surface. The poly(DMAEMA) brushes were further quaternized with methyl iodide. The resulting rod-like CNC-*g*-P(QDMAEMA) particles were characterized according to their chemical composition, surface charge properties and morphology, proving the presence of a thoroughly cationic polymer brush on the CNCs and the colloidal stability of the product. The CNC-*g*-P(QDMAEMA) were shown to bind CCMV and NoV-VLP with high affinities at different salt concentrations forming micrometer-sized virus-coated assemblies in solution. Additionally, the CNC-*g*-P(QDMAEMA) allowed the concentration of virus particles from solution by low-speed centrifugation. This original concept is widely applicable to other viruses and anionic materials such as DNA, bacteria and synthetic nanoparticles, and highly promising for enhancing the viral delivery of therapeutic agents.

Acknowledgements

Niklas Kähkönen is thanked for technical help with NoV-VLP preparation. Sami-Pekka Hirvonen (Laboratory of Polymer

Chemistry, University of Helsinki) is thanked for help with GPC measurements. Academy of Finland (projects: 273645, 267497), Emil Aaltonen Foundation and European Research Council Advanced Grant Mimefun are acknowledged for funding. This work was partially supported by the Academy of Finland under Center of Excellence in Molecular Engineering of Biosynthetic Hybrid Materials Research and made use of the facilities of Aalto University Nanomicroscopy Center (Aalto-NMC) premises.

Notes and references

[a]Molecular Materials, Department of Applied Physics, Aalto University, P.O. Box 15100, FI-00076 Aalto, Espoo, Finland.
[b]Department of Forest Products Technology, Aalto University, P.O. Box 16300, FI-00076 Aalto, Espoo, Finland.
[c]BioMediTech, University of Tampere, Biokatu 6, FI-33014 Tampere, Finland.
[d] Fimlab Laboratories, Biokatu 4, FI-33520 Tampere, Finland.
[e]Biohybrid Materials, Department of Biotechnology and Chemical Technology, Aalto University, FI-00076 Aalto, Espoo, Finland.

† Electronic Supplementary Information (ESI) available: CNC surface chain fraction and degree of substitution after BriBBr modification, NMR spectra of SI-ATRP reaction mixture at 0 and 120 min, conversion of DMAEMA monomer during SI-ATRP, DLS size distribution profiles of CNCs and CNC-*g*-P(QDMAEMA), TEM images of NoV-VLPs and their complexes with CNC-*g*-P(QDMAEMA) at 0 mM NaCl. See DOI: 10.1039/b000000x/

1 S. J. Eichhorn, A. Dufresne, M. Aranguren, N. E. Marcovich, J. R. Capadona, S. J. Rowan, C. Weder, W. Thielemans, M. Roman, S. Renneckar, W. Gindl, S. Veigel, J. Keckes, H. Yano, K. Abe, M. Nogi, A. N. Nakagaito, A. Mangalam, J. Simonsen, A. S. Benight, A. Bismarck, L. A. Berglund and T. Peijs, *J. Mater. Sci.*, 2010, **45**, 1-33.

2 Y. Habibi, L. A. Lucia and O. J. Rojas, *Chem. Rev.*, 2010, **110**, 3479-3500.

3 R. J. Moon, A. Martini, J. Nairn, J. Simonsen and J. Youngblood, *Chem. Soc. Rev.*, 2011, **40**, 3941-3994.

4 J. F. Revol, H. Bradford, J. Giasson, R. H. Marchessault and D. G. Gray, *Int. J. Biol. Macromol.*, 1992, **14**, 170-172.

5 V. Favier, G. R. Canova, S. C. Shrivastava and J. Y. Cavaillé, *Polym. Eng. Sci.*, 1997, **37**, 1732-1739.

6 J. R. Capadona, O. van den Berg, L. A. Capadona, M. Schroeter, S. J. Rowan, D. J. Tyler and C. Weder, *Nat. Nanotechnol.*, 2007, **2**, 765-769.

7 M. Pääkkö, J. Vapaavuori, R. Silvennoinen, H. Kosonen, M. Ankerfors, T. Lindström, L. A. Berglund and O. Ikkala, *Soft Matter*, 2008, **4**, 2492-2499.

8 H. Rosilo, E. Kontturi, J. Seitsonen, E. Kolehmainen and O. Ikkala, *Biomacromolecules*, 2013, **14**, 1547-1554.

9 J. R. McKee, E. A. Appel, J. Seitsonen, E. Kontturi, O. A. Scherman and O. Ikkala, *Adv. Funct. Mater.*, 2014, **24**, 2706–2713.

10 S. Dong, A. A. Hirani, K. R. Colacino, Y. W. Lee and M. Roman, *Nano LIFE*, 2012, **02**, 1241006/1241001-1241006/1241011.

11 A. P. Mangalam, J. Simonsen and A. S. Benight, *Biomacromolecules*, 2009, **10**, 497-504.

12 K. Fleming, D. Gray, S. Prasannan and S. Matthews, *J. Am. Chem. Soc.*, 2000, **122**, 5224-5225.

13 J. O. Zoppe, V. Ruottinen, J. Ruotsalainen, S. Rönkkö, L.-S. Johansson, A. Hinkkanen, K. Järvinen and J. Seppälä, *Biomacromolecules*, 2014, **15**, 1534–1542.

14 F. Fayazpour, B. Lucas, C. Alvarez-Lorenzo, N. N. Sanders, J. Demeester and S. C. De Smedt, *Biomacromolecules*, 2006, **7**, 2856-2862.

15 M. Andresen, P. Stenstad, T. Møretrø, S. Langsrud, K. Syverud, L.-S. Johansson and P. Stenius, *Biomacromolecules*, 2007, **8**, 2149-2155.

16 Y. B. Song, Y. X. Sun, X. Z. Zhang, J. P. Zhou and L. N. Zhang, *Biomacromolecules*, 2008, **9**, 2259-2264.

17 Y. B. Song, L. Z. Zhang, W. P. Gan, J. P. Zhou and L. N. Zhang, *Colloids Surf., B*, 2011, **83**, 313-320.

18 K. Roemhild, C. Wiegand, U.-C. Hipler and T. Heinze, *Macromol. Rapid Commun.*, 2013, **34**, 1767-1771.

19 M. Hasani, E. D. Cranston, G. Westman and D. G. Gray, *Soft Matter*, 2008, **4**, 2238-2244.

20 H. de la Motte, M. Hasani, H. Brelid and G. Westman, *Carbohydr. Polym.*, 2011, **85**, 738-746.

21 M. Zaman, H. N. Xiao, F. Chibante and Y. H. Ni, *Carbohydr. Polym.*, 2012, **89**, 163-170.

22 S. Beck and J. Bouchard, *Nord. Pulp Pap. Res. J.*, 2014, **29**, 6-14.

23 S. Eyley and W. Thielemans, *Chem. Commun.*, 2011, **47**, 4177-4179.

24 L. Jasmani, S. Eyley, R. Wallbridge and W. Thielemans, *Nanoscale*, 2013, **5**, 10207-10211.

25 E. Feese, H. Sadeghifar, H. S. Gracz, D. S. Argyropoulos and R. A. Ghiladi, *Biomacromolecules*, 2011, **12**, 3528-3539.

26 J. O. Zoppe, M. Österberg, R. A. Venditti, J. Laine and O. J. Rojas, *Biomacromolecules*, 2011, **12**, 2788-2796.

27 K. H. M. Kan, J. Li, K. Wijesekera and E. D. Cranston, *Biomacromolecules*, 2013, **14**, 3130-3139.

28 G. Morandi and W. Thielemans, *Polym. Chem.*, 2012, **3**, 1402-1407.

29 P. van de Wetering, N. J. Zuidam, M. J. van Steenbergen, O. A. G. J. van der Houwen, W. J. M. Underberg and W. E. Hennink, *Macromolecules*, 1998, **31**, 8063-8068.

30 A. Waly, F. A. Abdel-Mohdy, A. S. Aly and A. Hebeish, *J. Appl. Polym. Sci.*, 1998, **68**, 2151-2157.

31 X. Sui, J. Yuan, M. Zhou, J. Zhang, H. Yang, W. Yuan, Y. Wei and C. Pan, *Biomacromolecules*, 2008, **9**, 2615-2620.

32 D. Roy, J. S. Knapp, J. T. Guthrie and S. Perrier, *Biomacromolecules*, 2008, **9**, 91-99.

33 Q. Yan, J. Y. Yuan, F. B. Zhang, X. F. Sui, X. M. Xie, Y. W. Yin, S. F. Wang and Y. Wei, *Biomacromolecules*, 2009, **10**, 2033-2042.

34 F. J. Xu, Y. Ping, J. Ma, G. P. Tang, W. T. Yang, J. Li, E. T. Kang and K. G. Neoh, *Bioconjugate Chem.*, 2009, **20**, 1449-1458.

35 L. Ma, R. Liu, J. Tan, D. Wang, X. Jin, H. Kang, M. Wu and Y. Huang, *Langmuir*, 2010, **26**, 8697-8703.

36 H. Parviainen, M. Hiltunen and S. L. Maunu, *J. Appl. Polym. Sci.*, 2014, DOI: 10.1002/app.40448. Published online January 40431, 42014.

37 S. B. Lee, R. R. Koepsel, S. W. Morley, K. Matyjaszewski, Y. Sun and A. J. Russell, *Biomacromolecules*, 2004, **5**, 877-882.

38 B. V. Bhut, S. R. Wickramasinghe and S. M. Husson, *J. Membr. Sci.*, 2008, **325**, 176-183.

39 M. Jiang, J. Wang, L. Li, K. Pan and B. Cao, *RSC Advances*, 2013, **3**, 20625-20632.

40 J. Yi, Q. Xu, X. Zhang and H. Zhang, *Cellulose*, 2009, **16**, 989-997.

41 T. Douglas and M. Young, *Nature*, 1998, **393**, 152-155.

42 G. J. Tong, S. C. Hsiao, Z. M. Carrico and M. B. Francis, *J. Am. Chem. Soc.*, 2009, **131**, 11174-11178.

43 J. Mikkilä, A.-P. Eskelinen, E. H. Niemelä, V. Linko, M. J. Frilander, P. Törmä and M. A. Kostiainen, *Nano Lett.*, 2014, **14**, 2196-2200.

44 M. A. Kostiainen, P. Hiekkataipale, J. A. de la Torre, R. J. M. Nolte and J. J. L. M. Cornelissen, *J. Mater. Chem.*, 2011, **21**, 2112-2117.

45 X. Chen, K. Gerasopoulos, J. Guo, A. Brown, C. Wang, R. Ghodssi and J. N. Culver, *Adv. Funct. Mater.*, 2011, **21**, 380-387.

46 M. A. Kostiainen, P. Hiekkataipale, A. Laiho, V. Lemieux, J. Seitsonen, J. Ruokolainen and P. Ceci, *Nat. Nanotechnol.*, 2013, **8**, 52-56.

47 J. Mikkilä, H. Rosilo, S. Nummelin, J. Seitsonen, J. Ruokolainen and M. A. Kostiainen, *ACS Macro Lett.*, 2013, **2**, 720-724.

48 T. A. Ratko, J. P. Cummings, J. Blebea and K. A. Matuszewski, *Am. J. Med.*, 2003, **115**, 560-569.

49 H. E. Davis, M. Rosinski, J. R. Morgan and M. L. Yarmush, *Biophys. J.*, 2004, **86**, 1234-1242.

50 S. E. A. Gratton, P. A. Ropp, P. D. Pohlhaus, J. C. Luft, V. J. Madden, M. E. Napier and J. M. DeSimone, *Proc. Natl. Acad. Sci. U. S. A.*, 2008, **105**, 11613-11618.

51 M. Yolamanova, C. Meier, A. K. Shaytan, V. Vas, C. W. Bertoncini, F. Arnold, O. Zirafi, S. M. Usmani, J. A. Müller, D. Sauter, C. Goffinet, D. Palesch, P. Walther, N. R. Roan, H. Geiger, O. Lunov, T. Simmet, J. Bohne, H. Schrezenmeier, K. Schwarz, L. Standker, W. G. Forssmann, X. Salvatella, P. G. Khalatur, A. R. Khokhlov, T. P. J. Knowles, T. Weil, F. Kirchhoff and J. Münch, *Nat. Nanotechnol.*, 2013, **8**, 130-136.

52 E. Ten, C. Ling, Y. Wang, A. Srivastava, L. A. Dempere and W. Vermerris, *Biomacromolecules*, 2013, **15**, 327-338.

53 R. Wang, S. H. Guan, A. N. Sato, X. Wang, Z. Wang, R. Yang, B. S. Hsiao and B. Chu, *J. Membr. Sci.*, 2013, **446**, 376-382.

54 T. Serizawa, T. Sawada, H. Okura and M. Wada, *Biomacromolecules*, 2013, **14**, 613-617.

55 J. A. Speir, S. Munshi, G. Wang, T. S. Baker and J. E. Johnson, *Structure*, 1995, **3**, 63-78.

56 M. Herbst-Kralovetz, H. S. Mason and Q. Chen, *Expert Rev. Vaccines*, 2011, **9**, 299-307.

57 L. T. Lui, X. Xue, C. Sui, A. Brown, D. I. Pritchard, N. Halliday, K. Winzer, S. M. Howdle, F. Fernandez-Trillo, N. Krasnogor and C. Alexander, *Nat Chem*, 2013, **5**, 1058-1065.

58 C. D. Edgar and D. G. Gray, *Cellulose*, 2003, **10**, 299-306.

59 J. Majoinen, E. Kontturi, O. Ikkala and D. G. Gray, *Cellulose*, 2012, **19**, 1599-1605.

60 B. J. M. Verduin, *FEBS Lett.*, 1974, **45**, 50-54.

61 M. Comellas Aragonès, Doctoral dissertation, Radboud University Nijmegen, 2010.

62 T. Koho, L. Huhti, V. Blazevic, K. Nurminen, S. J. Butcher, P. Laurinmäki, N. Kalkkinen, G. Rönnholm, T. Vesikari, V. P. Hytönen and M. S. Kulomaa, *J. Virol. Methods*, 2012, **179**, 1-7.

63 T. Koho, T. Mäntylä, P. Laurinmäki, L. Huhti, S. J. Butcher, T. Vesikari, M. S. Kulomaa and V. P. Hytönen, *J. Virol. Methods*, 2012, **181**, 6-11.

64 P. A. Suci, D. L. Berglund, L. Liepold, S. Brumfield, B. Pitts, W. Davison, L. Oltrogge, K. O. Hoyt, S. Codd, P. S. Stewart, M. Young and T. Douglas, *Chem. Biol.*, 2007, **14**, 387-398.

65 J. Majoinen, A. Walther, J. R. McKee, E. Kontturi, V. Aseyev, J. M. Malho, J. Ruokolainen and O. Ikkala, *Biomacromolecules*, 2011, **12**, 2997-3006.

66 C. M. Hui, J. Pietrasik, M. Schmitt, C. Mahoney, J. Choi, M. R. Bockstaller and K. Matyjaszewski, *Chem. Mater.*, 2014, **26**, 745-762.

67 M. Ejaz, S. Yamamoto, K. Ohno, Y. Tsujii and T. Fukuda, *Macromolecules*, 1998, **31**, 5934-5936.

68 R. Konecny, J. Trylska, F. Tama, D. Zhang, N. A. Baker, C. L. Brooks and J. A. McCammon, *Biopolymers*, 2006, **82**, 106-120.

69 A. K. da Silva, O. V. Kavanagh, M. K. Estes and M. Elimelech, *Environ. Sci. Technol.*, 2011, **45**, 520-526.

70 J. C. Burns, T. Friedmann, W. Driever, M. Burrascano and J. K. Yee, *Proc. Natl. Acad. Sci. U. S. A.*, 1993, **90**, 8033-8037.

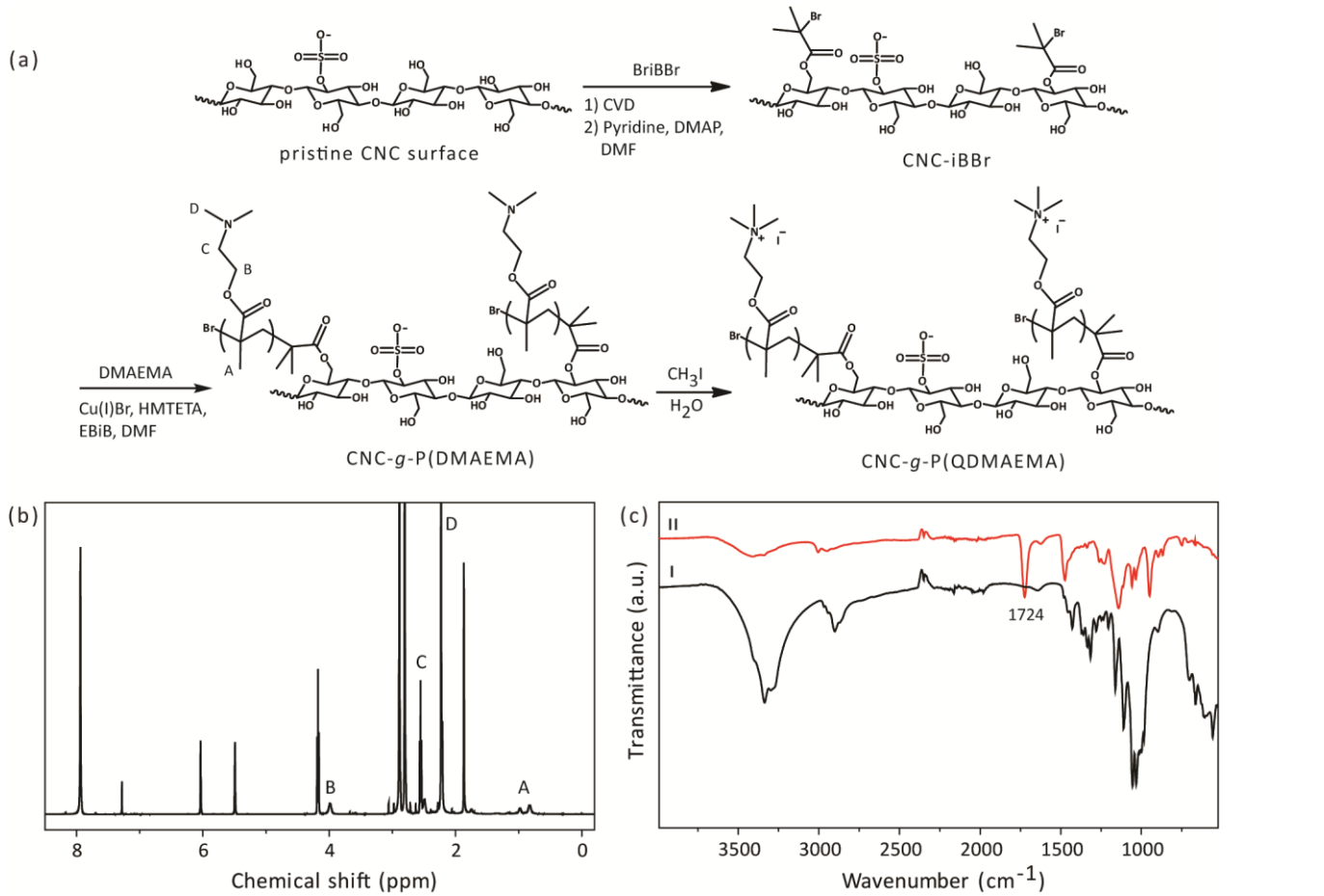

Fig. 1 (a) Reaction scheme for CNC surface modification including the two-step initiator modification, SI-ATRP of DMAEMA and quaternization of poly(DMAEMA) grafts on the CNCs. The letters A-D by the poly(DMAEMA) refer to the signals of the ^{1}H NMR spectrum. (b) ^{1}H NMR spectrum of the SI-ATRP reaction mixture after 240 minutes. (c) FTIR spectra for pristine CNCs and CNC-*g*-P(QDMAEMA) (I and II, respectively).

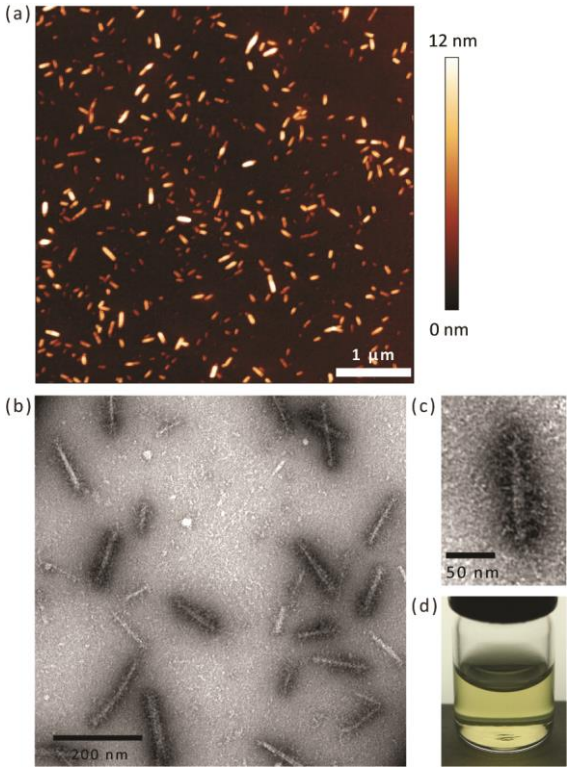

Fig. 2 (a) AFM topography image of CNC-*g*-P(QDMAEMA) spin-coated on mica (0.5 mg/mL in water). (b) and (c) TEM images of CNC-*g*-P(QDMAEMA) (0.1 mg/mL in water) negatively stained with uranyl acetate. (d) Photograph of a dispersion of CNC-*g*-P(QDMAEMA) in water (5 mg/mL).

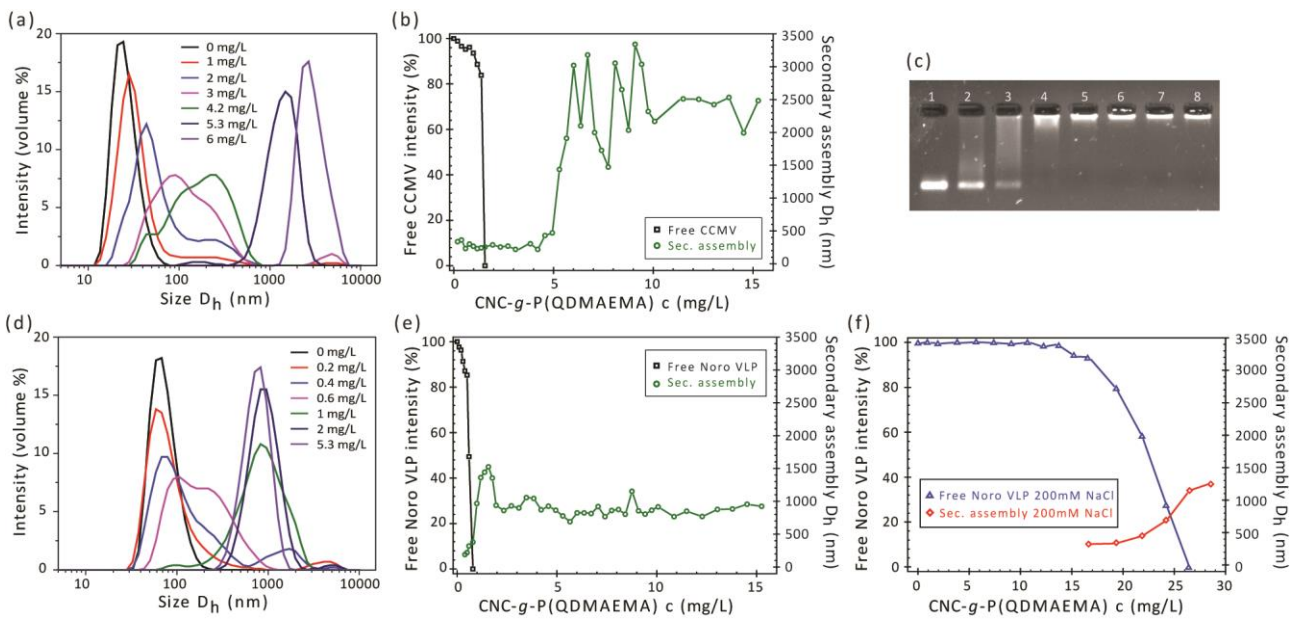

Fig. 3 (a) DLS results showing the change in the volume-averaged size distribution profile when CCMV solution was titrated with CNC-*g*-P(QDMAEMA). (b) DLS results presenting the changes in free CCMV scattering intensity and the secondary assembly size, when CCMV solution was titrated with CNC-*g*-P(QDMAEMA). (c) Gel electrophoresis of CCMV and CNC-*g*-P(QDMAEMA) complexes. Concentration of CCMV on each lane was 50 mg/L and concentration of CNC-*g*-P(QDMAEMA) was: lane 1: 0 mg/L, lane 2: 2.5 mg/L, lane 3: 5 mg/L, lane 4: 7.5 mg/L, lane 5: 10 mg/L, lane 6: 12.5 mg/L, lane 7: 15 mg/L and lane 8: 20 mg/L. (d) DLS results showing the change in the volume-averaged size distribution profile when NoV-VLP solution was titrated with CNC-*g*-P(QDMAEMA) in the absence of salt. (e, f) DLS results presenting the changes in free NoV-VLP scattering intensity and the secondary assembly size, when NoV-VLP solution was titrated with CNC-*g*-P(QDMAEMA) at (e) 0 mM NaCl and (f) 200 mM NaCl.

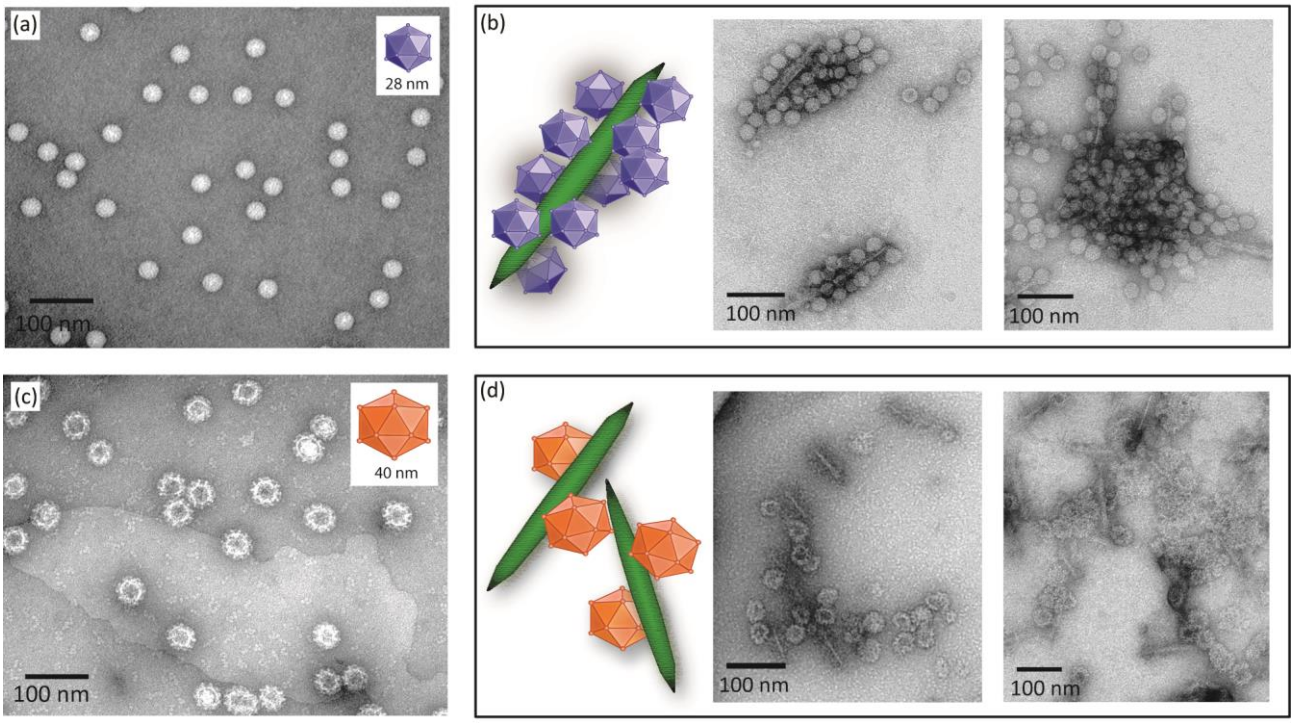

Fig. 4 TEM micrographs of CCMV and NoV-VLP and their complexes with CNC-*g*-P(QDMAEMA). All samples were negatively stained with uranyl acetate. (a) CCMV viruses in water. (b) Complexes of CNC-*g*-P(QDMAEMA) and CCMV in water. (c) NoV-VLP in 500 mM NaCl stock solution. (d) Complexes of CNC-*g*-P(QDMAEMA) and NoV-VLP at 200 mM NaCl.

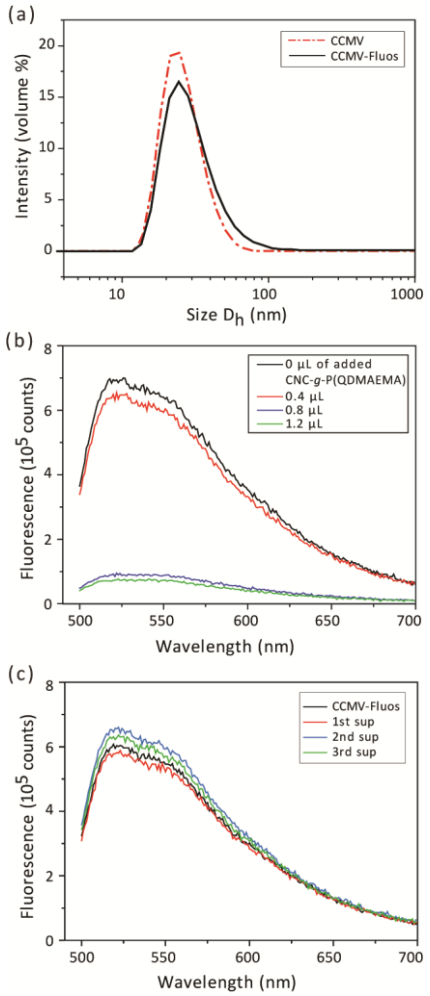

Fig. 5 (a) DLS results showing the volume-averaged size distribution profile of CCMV and CCMV-Fluos. (b) Fluorescence spectra of CCMV-Fluos and the recovered supernatants after CNC-*g*-P(QDMAEMA) additions and centrifugations. (c) Fluorescence spectra of CCMV-Fluos and the recovered supernatants (sup) after centrifugations.